AIAA Guidance, Navigation, and Control Conference
10 - 13 August 2009, Chicago, Illinois

AIAA 2009-6203

Analysis of Spinning Spacecraft with Wire Booms Part 2: Out-of-Plane Dynamics and Maneuvers

Timothy G. McGee*, Uday J. Shankar†, and Brian L. Kemp‡
Johns Hopkins University Applied Physics Laboratory
Laurel, MD, 20723, USA

An analysis of the dynamics for a spin stabilized spacecraft consisting of a rigid central hub with four long flexible wire booms is presented. The analysis focuses on the dynamics out of the spin plane of the spacecraft. Companion papers will focus on the derivations of the full nonlinear dynamics and analysis of the in plane dynamics. A linear analysis is used to estimate the mode shapes of the free response of the system, the effects of various damping mechanisms on these modes, and the dynamic response of the system to various maneuvers. The results of an independent simulation of the full nonlinear dynamics of the system are also provided to support the linear analysis. While the dynamics and analysis approach presented can be applied to the general class of spin stabilized spacecraft having multiple flexible wire booms, the numeric parameters studied represent those of the satellites from the Radiation Belt Storm Probe (RBSP) mission. The mission, part of NASA's Living With a Star Geospace Program, will launch two Earth-orbiting spacecraft to investigate how populations of relativistic electrons and ions in the region known as the Radiation Belts are formed and change in response to variable inputs of energy from the Sun.

Nomenclature

J_{ii}	Spacecraft hub moments of inertia, $kg \cdot m^2$
J_{ndi}	Nutation damper moment of inertia, $kg \cdot m^2$
J_{tot}	Total moment of inertia around spin axis, $kg \cdot m^2$
m_{hub}	Mass of the spacecraft hub, kg
m_i	Equivalent mass of boom i, kg
m_{tot}	Total mass of spacecraft, kg
b	Boom attachment radius, m
L_i	Boom equivalent length, m
θ_b	Boom offset angle from primary axis, rad
Ω	Spacecraft spin rate around z axis, rad/s
ω_i	Perturbed rotation around axis i
ϕ_i	Out of plane boom angle, rad
η_{ndi}	Rotation angle of nutation damper, rad
c_b	Boom equivalent viscous damping, $N \cdot m \cdot s$
c_{ndi}	Nutation damper viscous damping, $N \cdot m \cdot s$
τ_i	Actuator torques on spacecraft, $N \cdot m$
f_i	Actuator forces on spacecraft, N
s	Laplace variable

*Senior Professional Staff, Mission Design Guidance and Control, Space Department, AIAA Member.
†Senior Professional Staff, Mission Design Guidance and Control, Space Department, AIAA Associate Fellow.
‡Principal Professional Staff, Precision Engagement Systems, Global Engagement Department, AIAA Member.

I. Introduction

Flexible appendages have long been used on spacecraft as a means of allowing larger distances between sensors with minimal mass increase. One of the major engineering trades with this design approach, however, is that the large, low mass structures often introduce flexibility into the system that can result in increased oscillations. Spacecraft with wire boom structures are often spin stabilized to provide both pointing stability and increased stiffness by creating tension in the wire booms. An analysis is presented for the linearized dynamics of one such spacecraft which is spin stabilized and consists of a rigid central hub with four long flexible wire booms. This paper focuses on the dynamics out of the spin plane of the spacecraft. Companion papers will focus on the derivation of the full nonlinear dynamics and analysis of the in-plane dynamics.[1,2] Although the in-plane and out-of-plane dynamics are coupled in the full nonlinear dynamic equations of the system, they are decoupled in the linearized system. The four boom configuration has been presented in past studies,[3,4] although the calculated mode shapes in this study differ from those in the previous studies. It is believed that these discrepancies result from simplifying assumptions during the derivation of the modal dynamics in past four wire boom studies. The linearized dynamics presented in this paper agree with the linearized dynamics presented in a prior study on a similar configuration with only two wire booms.[5] In addition to identifying the mode shapes of the free response of the system, this study also investigates various damping mechanisms in the system and the dynamic response of the system to various maneuvers. Simulation results using the full nonlinear dynamics of the system are also provided to support all of the results of the linear analysis.

While the dynamics and analysis approach presented can be applied to the general class of spin stabilized spacecraft with flexible wire booms, the numeric parameters used in this paper represent those of the satellites from the Radiation Belt Storm Probe (RBSP) mission. The mission, part of NASA's Living With a Star Geospace Program, will launch two Earth-orbiting spacecraft to investigate how populations of relativistic electrons and ions in the region known as the Radiation Belts are formed and change in response to variable inputs of energy from the Sun. In addition to the primary science objectives, space weather data will be broadcast nearly continuously over the mission. Since adverse space weather and radiation are hazardous to astronauts, orbiting satellites, and aircraft flying high polar routes, the knowledge provided by this mission has the potential for real world engineering improvements in addition to purely scientific knowledge.

II. Dynamic Model Formulation

The spacecraft layout is illustrated in Figure 1. The wire booms lengths are shown to scale in the left image. The length of the wire booms allow larger separation of boom-tip mounted sensors. Assumptions used to model various components of the spacecraft including the rigid hub, flexible booms, and nutation dampers are presented in this section. Fuel slosh is not considered in this model. A Cartesian coordinate system is defined with its origin at the center of mass of the central hub. The three axes are aligned with the principal inertia axes of the central hub, with the z axis in the nominal direction of spacecraft rotation.

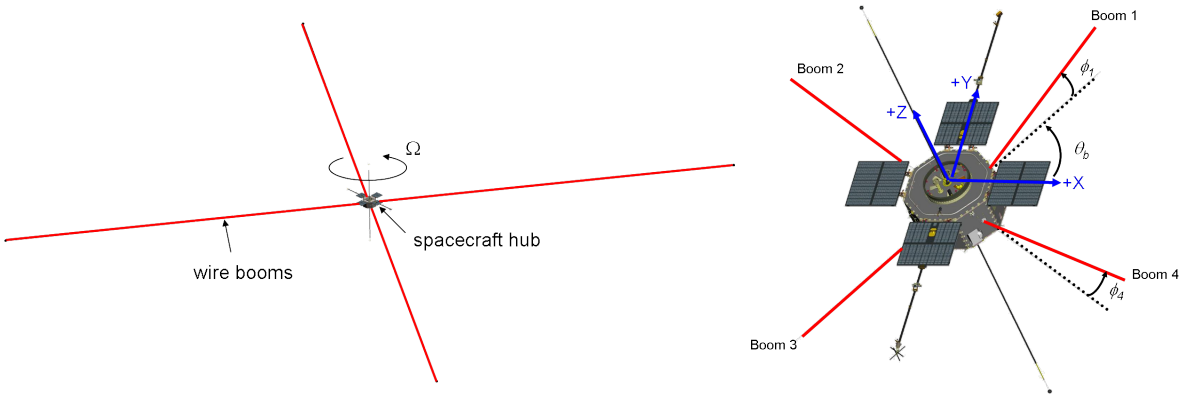

Figure 1. Spacecraft Layout

A. Spacecraft Configuration

The spacecraft system under consideration is a rigid central hub with four long flexible wire booms. The mass of the central hub is much larger than the mass in the wire booms. However, the length of the booms make their rotational inertia contribution nontrivial. In the case of the RBSP parameters, the inertia of the wire booms are larger than the rotational inertia of the hub. The RBSP spacecraft will also have other flexible structures including solar panels and other sensor booms attached to the central body. The effects of these flexible structures on the dynamics of the overall spacecraft are not considered in this analysis. The four wire booms are assumed to be equally spaced around the hub, but can be rotated by an angle θ_b relative to the principal inertia axes of the hub.

B. Boom Model

Two assumptions are made to simplify the analytical expressions for the wire booms. First, it is assumed that oscillations along the length of the boom are negligible. The booms can thus be modeled as a rigid link with a single rotation point at the connection to the hub. Second, each boom link is modeled by a massless rod of length L_{eq} and point tip mass m_{eq}. Because an actual boom will have distributed mass along its length from the density per length of the wire, ρ, and possible multiple point masses along its length, m_{eq} and L_{eq} are chosen to preserve the first and second mass moments of inertia of each boom around its rotation point. In order to preserve the mass of the boom, a second mass, m_{root}, can also be added at the connection point, although for the spacecraft under consideration the root mass is negligible. The validity of both of these assumptions was confirmed by the results of higher fidelity nonlinear simulation which modeled distributed mass and flexibility along the length of the boom.

$$\begin{aligned} m_{eq}L_{eq} &= \int \rho L dL \\ m_{eq}L_{eq}^2 &= \int \rho L^2 dL \\ m_{root} + m_{eq} &= \int \rho dL \end{aligned} \tag{1}$$

C. System Damping

The three most common analytical damping models are viscous, coulomb, and hysteretic. The viscous damping model is common for systems with fluids, where the torque, τ_{damp}, is proportional to rate, $\dot{\theta}$, and a constant, c_{visc}, that is independent of frequency.

$$\tau_{damp} = c_{visc}\dot{\theta} \tag{2}$$

Coulomb damping represents rubbing surfaces, where torque is constant in magnitude but opposes velocity. The magnitude of this torque, τ_{coul}, is typically proportional to the normal force between the rubbing surfaces.

$$\tau_{damp} = \tau_{coul} sign\left(\dot{\theta}\right) \tag{3}$$

Hysteretic damping characterizes damping in solid materials, where the damping force behaves like a complex spring. The energy dissipated per cycle by hysteretic damping is independent of the frequency, $\bar{\omega}$.

$$\tau_{damp} = j h_{hyst} sign(\bar{\omega})\theta \tag{4}$$

While the hysteretic damping model in Eq. 4 is easily applied to a forced response at a known frequency, it has a non causal impulse response and thus poses problems for use in free response calculations.[6,7] In order to deal with this problem, the mode frequencies were first calculated for the undamped system. With the known frequencies, the hysteric model in Eq. 4 can be approximated using an equivalent viscous damping model.

$$\tau_{damp} = \frac{h_{hyst}}{|\bar{\omega}|}\dot{\theta} = c_{eq}\dot{\theta} \tag{5}$$

1. Boom Damping

One damping mechanism in the system is the inherent damping in the booms themselves as they bend at connection point. The nature of the damping in the wire used for the RBSP spacecraft was studied using experimental data from a team at the University of California, Berkeley which measured the decay of oscillations of a pendulum of the boom material in a vacuum chamber. From these tests, it appears that the total damping in the wires is a combination of hysteretic and coulomb friction, although the coulomb friction appears to drop off significantly at boom angles less than a few degrees. Since, as will be illustrated later in the study, all of the mode shapes which are primarily damped by boom damping have frequencies close to the spin rate, Ω, the hysteretic damping can be replaced by a single viscous damper using Eq. 5. While test data indicated coulomb damping at higher amplitudes, it is ignored in this study since it cannot be accounted for easily using linear analysis. The equivalent viscous damping, however, is chosen conservatively so that any additional coulomb damping would merely decrease decay times.

2. Nutation Damper

Nutation dampers in the form of fluid-filled rings are to be added to the central hub. The damping effects of the rotating fluid in the ring are modeled by a rotating rigid disc connected to the hub by a viscous damper that exerts a torque proportional to the rotation rate between the disc and the spacecraft hub. The proper sizing and modeling parameters of the damper can be calculated from the physical properties of the fluid used and the desired damping.[8,9] Given the volume constraints in the RBSP hub structure, there will be two separate rings that together provided the desired amount of damping. One ring is parallel to the y-z plane of the spacecraft body with the x axis through the center of the ring, and the second ring is parallel to the x-z plane with the y axis running through its center. The dynamics model includes each ring separately to better reflect the spacecraft design although an equivalent effect could be obtained with a single larger disc.

D. Linearized Equations of Motion

The spacecraft equations of motion were linearized around the equilibrium point defined by a nominal spin rate, Ω, around the z axis of the spacecraft with zero nutation and no displacement angles in the booms. The formulation of the dynamics presented below was found independently from the full nonlinear dynamics described in Part 1 of the paper, using a combination of Newtonian dynamics for the hub motion and Lagrangian dynamics for individual wire boom motion. The independent derivations were found to be equivalent, however. After linearization, it was found that the dynamics could be decoupled into in-plane and out-of-plane dynamics. The out-of-plane equations of motion are represented by nine configuration parameters, z, ω_x, ω_y, ϕ_1, ϕ_2, ϕ_3, ϕ_4, η_{nd1}, and η_{nd2}. The first parameter z is the displacement of the center of mass of the hub perpendicular to the spin plane. The second two parameters, ω_x and ω_y, are the rotation rates of the hub in its body-fixed frame. The body rates are used in order to avoid the use of Euler angles or quaternions that can complicate the linear analysis. The four ϕ_i values are the angles between each boom and the $x-y$ plane of the hub. The two η_{ndi} values are the angles of rotation of the nutation damper discs relative to the spacecraft hub around their rotation axes. These nine parameters can be combined into a single vector, x:

$$x = \begin{bmatrix} z & \omega_x & \omega_y & \phi_1 & \phi_2 & \phi_3 & \phi_4 & \eta_{nd1} & \eta_{nd2} \end{bmatrix}^T \tag{6}$$

Although x is not a state vector of the system because it doesn't uniquely define the state of the system in inertial space, it will be quite useful for describing the equations of motion and calculating oscillatory modes in the system. Using the vector, x, the linearized dynamics can be defined in the form:

$$A_1\ddot{x} + A_2\dot{x} + A_3 x = f \tag{7}$$

where A_1, A_2, and A_3 are matrices depending on the physical properties of the system. These matrices are slightly different than standard mass, damping, and stiffness matrices since the vector x contains both position and velocity terms. The vector f is comprised of out of plane actuator forces on the hub including the axial force, f_z and torques, τ_x and τ_y in the body-fixed frame:

$$f = \begin{bmatrix} f_z & \tau_x & \tau_y & 0 & 0 & 0 & 0 & 0 & 0 \end{bmatrix}^T \tag{8}$$

Taking the Laplace transform of Eq. 7, the dynamics can be expressed more compactly in the form:

$$[A_1 s^2 + A_2 s + A_3]X = A_{dyn}(s)X = F \tag{9}$$

This formulation of the dynamics is also useful for analytical analysis. The complete description of A_{dyn} is given below in Eq. 10-19.

$$A_{dyn}X = \begin{bmatrix} A_{hh} & A_{bh} & A_{dh} \\ A_{hb} & A_{bb} & 0 \\ A_{hd} & 0 & A_{dd} \end{bmatrix} \begin{Bmatrix} Z \\ \Omega_x \\ \Omega_y \\ \Phi_1 \\ \Phi_2 \\ \Phi_3 \\ \Phi_4 \\ H_{nd1} \\ H_{nd2} \end{Bmatrix} = \begin{bmatrix} F_z \\ T_x \\ T_y \\ 0 \\ 0 \\ 0 \\ 0 \\ 0 \\ 0 \end{bmatrix} = F \tag{10}$$

$$\begin{bmatrix} Z & \Omega_x & \Omega_y & \Phi_1 & \Phi_2 & \Phi_3 & \Phi_4 & H_{nd1} & H_{nd2} \end{bmatrix}^T = \mathcal{L}\left(\begin{bmatrix} z & \omega_x & \omega_y & \phi_1 & \phi_2 & \phi_3 & \phi_4 & \eta_{nd1} & \eta_{nd2} \end{bmatrix}^T \right) \tag{11}$$

$$\begin{bmatrix} F_z & T_x & T_y & 0 & 0 & 0 & 0 & 0 & 0 \end{bmatrix}^T = \mathcal{L}\left(\begin{bmatrix} f_z & \tau_x & \tau_y & 0 & 0 & 0 & 0 & 0 & 0 \end{bmatrix}^T \right) \tag{12}$$

$$A_{hh} = \begin{bmatrix} m_{tot}s^2 & 0 & 0 \\ 0 & s(J_{xx} + J_{nd2}/2) & \Omega(J_{zz} - J_{yy} - J_{nd2}/2)) \\ 0 & \Omega(J_{xx} - J_{zz} + J_{nd2}/2) & s(J_{yy} + J_{nd2}/2)) \end{bmatrix} \tag{13}$$

$$A_{bh} = \begin{bmatrix} m_1 L_1 s^2 & m_2 L_2 s^2 & m_3 L_3 s^2 & m_4 L_4 s^2 \\ -(m_1 b(b+L_1)\Omega^2 + c_b s)\sin\theta_b & -(m_2 b(b+L_2)\Omega^2 + c_b s)\cos\theta_b & (m_3 b(b+L_3)\Omega^2 + c_b s)\sin\theta_b & (m_4 b(b+L_4)\Omega^2 + c_b s)\cos\theta_b \\ (m_1 b(b+L_1)\Omega^2 + c_b s)\cos\theta_b & -(m_2 b(b+L_2)\Omega^2 + c_b s)\sin\theta_b & -(m_3 b(b+L_3)\Omega^2 + c_b s)\cos\theta_b & (m_4 b(b+L_4)\Omega^2 + c_b s)\sin\theta_b \end{bmatrix} \tag{14}$$

$$A_{dh} = \begin{bmatrix} 0 & 0 \\ -c_{nd1}s & -\Omega J_{nd2}s \\ \Omega J_{nd1}s & -c_{nd2}s \end{bmatrix} \tag{15}$$

$$A_{hb} = \begin{bmatrix} s^2 & (L_1+b)(\Omega\cos\theta_b + s\sin\theta_b) & (L_1+b)(\Omega\sin\theta_b - s\cos\theta_b) \\ s^2 & (L_2+b)(s\cos\theta_b - \Omega\sin\theta_b) & (L_2+b)(s\sin\theta_b + \Omega\cos\theta_b) \\ s^2 & (L_3+b)(-\Omega\cos\theta_b - s\sin\theta_b) & (L_3+b)(-\Omega\sin\theta_b + s\cos\theta_b) \\ s^2 & (L_4+b)(-s\cos\theta_b + \Omega\sin\theta_b) & (L_4+b)(-s\sin\theta_b - \Omega\cos\theta_b) \end{bmatrix} \tag{16}$$

$$A_{bb} = \begin{bmatrix} s^2L_1 + \Omega^2(b+L_1) \\ +c_b s/m_1 L_1 & 0 & 0 & 0 \\ 0 & s^2L_2 + \Omega^2(b+L_2) \\ & +c_b s/m_2 L_2 & 0 & 0 \\ 0 & 0 & s^2L_3 + \Omega^2(b+L_3) \\ & & +c_b s/m_3 L_3 & 0 \\ 0 & 0 & 0 & s^2L_4 + \Omega^2(b+L_4) \\ & & & +c_b s/m_4 L_4 \end{bmatrix} \tag{17}$$

$$A_{hd} = \begin{bmatrix} 0 & J_{nd1}s & 0 \\ 0 & 0 & J_{nd2}s \end{bmatrix} \tag{18}$$

$$A_{dd} = \begin{bmatrix} J_{nd1}s^2 + c_{nd1}s & 0 \\ 0 & J_{nd2}s^2 + c_{nd2}s \end{bmatrix} \tag{19}$$

III. Modal Analysis

Using the formulation of the dynamics given in Eq. 9, the modal frequencies of the system can be determined by solving the roots of the equation:

$$det(A_{dyn}(s)) = 0 \tag{20}$$

If there is no damping, the roots will be purely imaginary and correspond to the undamped frequencies of the modes. If there is damping, the real part of each root, s_i, will correspond to the damping of that mode, while the imaginary part will correspond to the damped frequency of the mode. The shape of each mode can be calculated as the null space of the matrix $A_{dyn}(s_i)$ using the value of s_i corresponding to the mode under consideration. The method described above is not the only approach to finding the frequencies and mode shapes. If an augmented vector is defined to include x and its derivatives, the modes could also be determined using eigenvalues and eigenvector analysis.

A. Undamped Mode Shapes: Symmetric Configuration

In order to better understand the mode shapes, a radially symmetric spacecraft was first studied with properties similar to the nominal RBSP parameters. The booms were assumed to be equal length using the average of the calculated lengths and masses from Eq. 1. The hub inertias around the x and y axes were chosen so that the hub nutation frequency of the center hub with no booms would be the same as the boomless hub of the actual spacecraft. Recall that for a rigid spacecraft spinning stably around its z axis, the nutation frequency can be calculated as:

$$\omega_{rig} = \Omega\sqrt{\frac{(I_{zz} - I_{xx})(I_{zz} - I_{yy})}{I_{xx}I_{yy}}} \tag{21}$$

Thus, for the symmetric case, a value I_{eq} was calculated so that for $I_{xx} = I_{yy} = I_{eq}$ the following equation would be satisfied.

$$\Omega\sqrt{\frac{(I_{zz} - I_{xx})(I_{zz} - I_{yy})}{I_{xx}I_{yy}}} = \Omega\frac{I_{zz} - I_{eq}}{I_{eq}} \tag{22}$$

The system parameters for the symmetric spacecraft configuration are listed in Table 1. Using these parameters, assuming no damping, the mode shapes and frequencies are listed in Table 2. The imaginary mode shapes for modes 3-5 indicate that the variables in the mode are out of phase with one another as a result of gyroscopic coupling. For an imaginary mode shape at frequency ω_i, the time response for an individual variable with mode amplitude $\alpha + \beta j$ can be viewed as:

Parameter	Value	Units
J_{xx}	349.7	$kg \cdot m^2$
J_{yy}	349.7	$kg \cdot m^2$
J_{zz}	491.7	$kg \cdot m^2$
m_{hub}	511.8	kg
b	0.962	m
L_i	38.02	m
m_i	0.231	kg
Ω	0.5236	rad/sec
θ	0	rad

Table 1. Symmetric Configuration Parameters

	Mode #	1	2	3	4	5
ω_i/Ω		1.0135	1.0126	1.0473	1.0131	0.4403
z	m	-0.069	0	0	0	0
ω_x	rad/sec	0	0	0.018	-0.043	-0.759
ω_y	rad/sec	0	0	$0.018j$	$0.043j$	$0.759j$
ϕ_1	rad	1	1	1	1	1
ϕ_2	rad	1	-1	j	$-j$	$-j$
ϕ_3	rad	1	1	-1	-1	-1
ϕ_4	rad	1	-1	$-j$	j	j

Table 2. Symmetric Configuration Undamped Mode Shapes

$$y_i(t) = Real\left[(\alpha + \beta j)e^{j\omega_i t}\right] = |\alpha + \beta j| cos\left(\omega_i t + atan2(\beta, \alpha)\right) \tag{23}$$

The first two mode shapes are fairly straight forward and involve only vertical translation of the hub and boom masses. The second three modes involve more complicated rotational motions. While the first two modes have been properly identified in past studies of four boom systems,[3,4] the frequencies and shapes of the gyroscopic modes have not been. In order to better visualize these three modes, it can be observed that the four boom angles are all 90 degrees out of phase with one another. Thus, for a pure modal response of one of the last three modes, the boom masses remain coplanar relative to one another. For visualization purposes, the four boom masses can thus be viewed as a solid hoop around the central hub. The modal shapes are illustrated in Fig. 2. For modes 3 through 5, the solid gray arrow represents the z axis of the central hub, and the solid black arrow represents the normal to the plane defined by the four boom masses. In each of the coupled modes, the spacecraft z axis and the boom plane normal vector trace out circles in inertial space around the constant angular momentum vector of the system. The frequency that these vectors precess in inertial space, ω_{Ii}, can be calculated from the mode frequency, ω_i and the spin rate of the spacecraft, Ω.

$$\omega_{I3} = \omega_3 - \Omega \tag{24}$$

$$\omega_{I4,5} = \omega_{4,5} + \Omega \tag{25}$$

The precession frequencies and periods for the symmetric configuration using Eqs. 24 and 25 are listed in Table 3. From the mode shapes and inertial precession frequencies, several more intuitive interpretations of the mode shapes can be made. For mode 3, since the inertial precession period is much slower than the spin rate, to first order, the boom plane and the body can each be viewed as rotating stably around their independent axes. The wires connecting the boom masses to the hub create a torque between the hub and the boom plane that is parallel to the cross product of the spacecraft z axis and the boom normal.

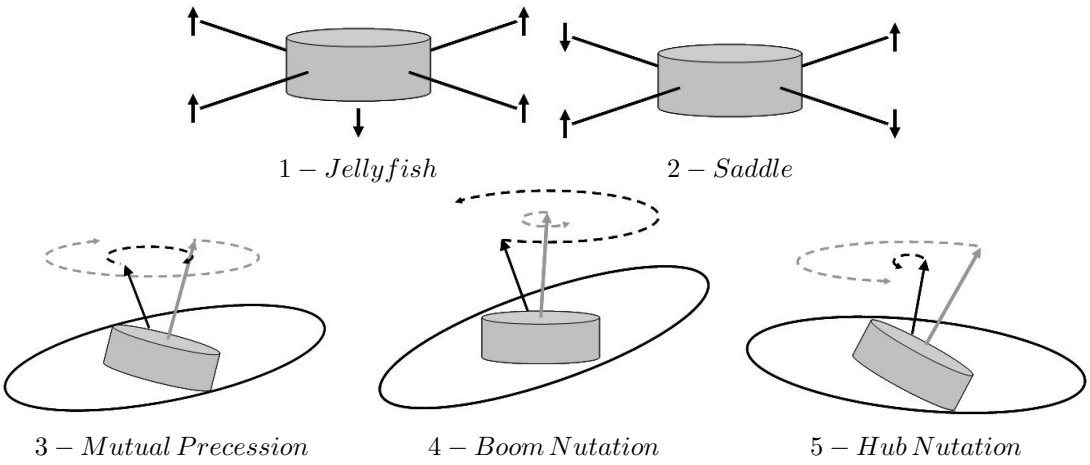

Figure 2. Mode Shapes for Symmetric Spacecraft

Mode	ω_{Ii} (rad/sec)	Period (sec)
3	0.0248	254
4	1.054	5.96
5	0.754	8.33

Table 3. Inertial Precession Frequencies and Periods

This interaction torque causes the hub and the boom plane to precess in opposite directions in inertial space. For mode 4, the motion can be approximately viewed as a rigid boom plane nutating on its own. A rigid symmetric disc has mass moments of inertia $I_{xx} = I_{yy} = I_{zz}/2$. From Eq. 21 it can be seen that a rigid symmetric disc would have a nutation frequency equal to the spin frequency Ω. For this mode, $\omega_4/\Omega = 1.0131 \approx 1.0$. Similarly, mode 5 can be approximately viewed as the central hub nutating on its own. From Eq. 21, the nutation frequency of the hub without booms can be calculated as 0.0406Ω, which is close to the value 0.0440Ω calculated for the mode.

B. Undamped Mode Shapes: Actual Configuration

The actual RBSP spacecraft is not symmetric. The spacecraft hub is not radially symmetric and the booms are not all the same length. More characteristic parameters are listed in Table 4. Using these parameters, the calculated mode shapes are listed in Table 5. It can be seen that the frequencies are nearly identical to the symmetric case and the mode shapes are qualitatively similar. There are some minor differences, however. For mode 1, the *jellyfish mode*, the four booms are in phase, but the two sets of opposing pairs have different amplitudes. For the *saddle mode*, the magnitudes of the boom oscillations are different for the long and short pairs and there is also a body translation not seen in the *saddle* mode of the symmetric case. The final three modes are also gyroscopically coupled modes similar to those illustrated in Fig. 2 although the spacecraft z axis and boom plane normal vector trace ellipses in inertial space instead of circles.

C. Damping Time Constant

When damping is added to the system, the damping for each mode is calculated along with the frequencies from Eq. 20. With damping, the frequency solutions will be of the form:

$$s_i = -\gamma_i \pm \omega_{di} j \tag{26}$$

Solutions of this form correspond to sinusoidal responses with exponential decay.

$$y(t) = Ae^{-\gamma_i t} cos(\omega_{di} t + \hat{\phi}_i) = Ae^{-t/tc_{di}} cos(\omega_{di} t + \hat{\phi}_i) \tag{27}$$

Parameter	Value	Units
J_{xx}	412.5	$kg \cdot m^2$
J_{yy}	264.6	$kg \cdot m^2$
J_{zz}	491.7	$kg \cdot m^2$
m_{hub}	511.8	kg
b	0.962	m
$L_{1,3}$	34.03	m
$m_{1,3}$	0.214	kg
$L_{2,4}$	42.01	m
$m_{2,4}$	0.238	kg
Ω	0.5236	rad/sec
θ	0.9599	rad

Table 4. Actual Configuration Parameters for RBSP Spacecraft

	Mode #	1	2	3	4	5
ω_i/Ω		1.0145	1.0118	1.0470	1.0135	0.4496
z	m	-0.033	0.15	0	0	0
ω_x	rad/sec	0	0	0.005 +0.002j	-0.024 - 0.033j	-0.722-0.533j
ω_y	rad/sec	0	0	0.029 +0.015j	-0.035+0.023j	-0.425 +0.564j
ϕ_1	rad	1	1	1	1	1
ϕ_2	rad	0.128	-4.62	-0.033+0.946j	0.008-0.784j	-0.660 -0.993j
ϕ_3	rad	1	1	-1	-1	-1
ϕ_4	rad	0.128	-4.62	0.033-0.946j	-0.008+0.784j	0.660+0.993j

Table 5. Actual Configuration Undamped Mode Shapes

Thus the time constant of the decay of a given mode, tc_{di}, can be calculated as:

$$tc_{di} = 1/\gamma_i \tag{28}$$

The damping performance was studied for the non-symmetric spacecraft configuration in Table 4. Two types of damping, viscous damping at the root of the booms and nutation ring dampers on the central hub were explored. The parameters for the damping properties are listed in Table 6 and the resulting damping time constants for each damping mechanism individually and together are listed in Table 7. The introduction of damping had a negligible effect on the vibration frequencies and mode shapes for this configuration. From these results, it can be seen that the nutation dampers mounted on the central hub are only effective in damping out mode 5, which is effectively hub only nutation. The nutation dampers had negligible damping on modes 3 and 4 and no effect on modes 1 and 2. The inherent damping in the booms, however, was able to damp all of the modes. Together, these results indicate that for the spacecraft configuration under consideration some boom damping between the body and the wire booms is required to provide reasonable damping for all of the modes.

IV. Out of Plane Maneuvers

The two expected spacecraft maneuvers which will excite the out of planes modes described above are axial ΔV thrusts along the spacecraft spin (z) axis and repointing of the spin axis. Both of these maneuvers are accomplished with thrusters on the spacecraft central hub which are oriented with thrust parallel to the z axis. There are four total out-of-plane thrusters planned for each RBSP spacecraft as illustrated in Fig. 3. Firing thrusters P1 and P2 together or P3 and P4 together will produce pure forces along the z axis. Firing thrusters P1 and P3 together or P2 and P4 together will produce positive or negative torques around an axis which lies in the $x - y$ axis of the spacecraft hub frame.

Parameter	Value	Units
J_{nd1}, J_{nd2}	0.1723	$kg \cdot m^2$
c_{nd1}, c_{nd2}	0.0874	$N \cdot m \cdot s$
c_b	0.016	$N \cdot m \cdot s$

Table 6. Damping Parameters

Mode #	1	2	3	4	5
ω_i/Ω	1.0145	1.0118	1.0470	1.0135	0.4496
nutation dampers	N/A	N/A	1030	170	1.7
boom damping	8.7	14.3	3.0	9.8	8.4
both	8.7	14.3	3.0	9.0	1.4

Table 7. Modal Damping Time Constants (hr)

For both types of maneuvers, the forces and torques applied to the spacecraft body can be modeled as known functions with respect to time. Taking the Laplace transform of these signals, the system dynamics can be put in the form of Eq. 20. The forced response can then be found by taking the inverse of the dynamics:

$$X = A_{dyn}^{-1} F \tag{29}$$

From this formulation, ignoring the damping components for clarity, the forced response for a single forcing frequency, ω_f, will be of the form:

$$X = \sum \left(\frac{B_{i^+}}{s - j\omega_i} + \frac{B_{i^-}}{s + j\omega_i} \right) + \left(\frac{B_{f^+}}{s - j\omega_f} + \frac{B_{f^-}}{s + j\omega_f} \right) \tag{30}$$

where the ω_i values are the modal frequencies of the free response, the B_i values are scaled mode shape vectors, ω_f is the forcing frequency and B_f is a mode shape at the forced frequency. The corresponding elements of the B_{i^+} and B_{i^-} vectors are complex conjugates and thus have identical magnitudes but opposite phases. The individual B_i values can be calculated by factoring the inversed dynamics:

$$B_{i^+} = \left| \frac{F_n(s) adj(A)(s - j\omega_i)}{(s^2 + \omega_f^2) \prod (s \pm j\omega_i)} \right|_{s = j\omega_i} \tag{31}$$

where $F_n(s)$ is the numerator of the Laplace transform of the forcing function at the given frequency and $adj(A)$ is the adjoint of matrix A. If the forcing function has multiple frequencies, each frequency can be treated separately using the approach above and the results summed. If the forcing function is not a sinusoidal input, the response can also have other terms of the form $1/s^n$ corresponding to steps, ramps and quadratic responses, but these will be ignored since they do not correspond to vibrations.

Once the B_i values are calculated, the time response for each mode can be reconstructed from the relationship:

$$|B_i[n]| \left(e^{j\omega_i t + \hat{\phi}_i[n]} + e^{-j\omega_i t - \hat{\phi}_i[n]} \right) = 2|B_i[n]| cos(\omega_i t + \hat{\phi}_i[n]) \tag{32}$$

where $|B_i[n]|$ and $\hat{\phi}_i[n]$ are the the magnitude and phase of the n^{th} element of the vector B_{i^+}.

A. Axial ΔV

An axial ΔV maneuver is done by firing two of the four thrusters along the spacecraft z axis, each with thrust f_p. Thus, the force on the body, $f_z(t)$ is a step function:

$$F_z(s) = \frac{2f_p}{s} \tag{33}$$

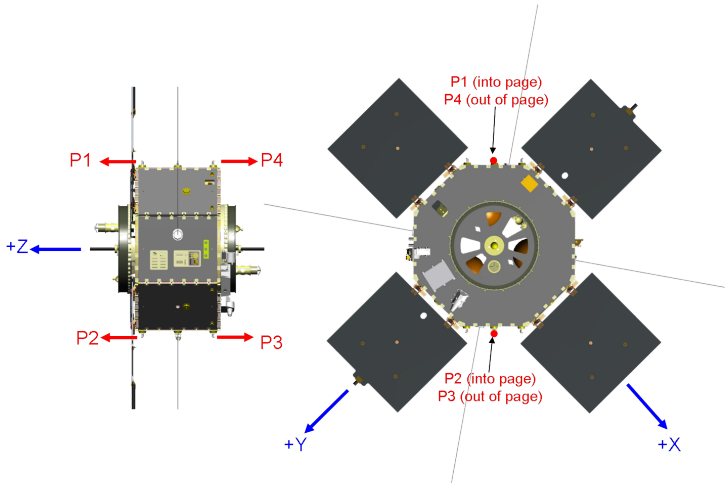

Figure 3. Out of Plane Thruster Layout

Parameter	Value	Units
f_p	1.07	N
L_p	1.007	m
f_z	2.14	N
τ_p	1.077	$N \cdot m$
θ_p	$\pi/2$	rad
τ_{avg}	0.485	$N \cdot m$

Table 8. Maneuver Forcing Parameters

For the RBSP spacecraft, the maximum force per thruster, shown in Table 8, is 1.07 N. This thrust value corresponds to the maximum thrust with full fuel tanks. The modal response from an axial ΔV using the RBSP properties is shown in Table 9. Since the maneuver is a pure thrust, only the first two modes are excited. The peak boom angles, ϕ_i, still remain very small, on the order of a few hundredths of a degree.

B. Repointing Maneuver

Repointing of the spacecraft spin axis is done using a standard Rhumb line maneuver.[10] This maneuver can visualized using a unit sphere with the spacecraft at the center. The sun vector is the "north pole" of the sphere. The spacecraft spin axis can be viewed as a ship on the surface of the sphere. The Rhumb line maneuver is the repositioning of the spin axis on this sphere by thrusting at a constant heading relative to the sun. Although a Rhumb line maneuver is not optimal with respect to fuel use unless travelling directly toward the sun, directly away from the sun, or along the equator, it is used because it can be performed by timing thruster pulses off of a sun sensor in order to produce torque in the desired direction relative to the sun. The majority of the repointing maneuvers planned for the RBSP spacecraft will be constant latitude maneuvers relative to the sun in order to maintain the angle between the sun and the spin axis within a desired range throughout the year.

The linear analysis above does not lend itself well to a completely accurate representation of a Rhumb line maneuver timed off of a sun pulse. However, there are two fairly straightforward ways to approximate the maneuver and capture the dominant dynamics. The first is to model the thrusting torque as a pulse train in a fixed direction in the body at the spin period of the spacecraft. This pulse train could then be approximated using the first several elements of its Fourier expansion that could be analyzed individually and

	Mode #	1	2	3	4	5
ω_i/Ω		1.0145	1.0118	1.0470	1.0135	0.4496
z	m	-1.7e-5	-9.5e-6	0	0	0
ω_x	rad/sec	0	0	0	0	0
ω_y	rad/sec	0	0	0	0	0
ϕ_1	rad	5.0e-4	-6.3e-5	0	0	0
ϕ_2	rad	6.4e-5	2.9e-4	0	0	0
ϕ_3	rad	5.0e-4	-6.3e-5	0	0	0
ϕ_4	rad	6.4e-5	2.9e-4	0	0	0

Table 9. Axial Thrust Maneuver Forced Response

then superimposed. A second approach is to approximate the pulse train with constant magnitude torque in the x-y plane of the spacecraft hub that is rotating at negative the spin rate, $-\Omega$, in the body frame. Since this torque rotates opposite the body spin rate, it can be viewed as a constant torque in the inertial frame. Although this second approach is more simplified, it was found to capture the dominant dynamics. For a perfect square pulse, the corresponding average torque, τ_{avg}, can be calculated from the magnitude of the torque pulse, τ_p, and the angle of rotation over which the pulse is on, θ_p.

$$\tau_{avg} = \frac{\tau_p \theta_p}{2\pi} \frac{\sin(\theta_p/2)}{\theta_p/2} = \frac{\tau_p \sin(\theta_p/2)}{\theta_p} \tag{34}$$

the $\sin(\theta/2)/(\theta/2)$ term accounts for efficiency losses from a finite pulse. Since the torque is applied with a coupled pair of thrusters, the pulse torque can be calculated from the thrust from one thruster, f_p, and the lever arm of the thruster, L_p.

$$\tau_p = 2 f_p L_p \tag{35}$$

In order to apply this rotating average torque in the body frame, it can be expressed in the Laplace domain as:

$$\begin{bmatrix} T_x \\ T_y \end{bmatrix} = \tau_{avg} \begin{bmatrix} \frac{s}{s^2+\Omega^2} \\ \frac{-\Omega}{s^2+\Omega^2} \end{bmatrix} \tag{36}$$

For the RBSP spacecraft, examples values for precession thrust are listed in Table 8. These values represent an upper bound on the expected precession torque assuming maximum tank pressure and the upper bound of potential pulse widths. The resulting response for these inputs is summarized in Table 10. The values in the table represent the magnitude and phase of the sinusoidal response for each variable in the multiple modes. As expected, modes 1 and 2 are not excited since they include translational oscillations, and the forcing function is a pure torque. The largest responses are in mode 3 and the forced frequency. Since the dominant responses in mode 3 and the spin frequency have amplitudes that are very close and are at very similar frequencies, they will produce a clear beating pattern as illustrated in Fig. 7. This beating could be used as a potential method of mitigating system oscillations after a repointing maneuver. The total maneuver time required, t_m, can be calculated from the total angular momentum of the spacecraft, the angle traced out by the angular momentum vector during the Rhumb Line maneuver, ϕ_m, and the average torque.

$$t_m = \frac{J_{tot} \Omega \phi_m}{\tau_{avg}} \tag{37}$$

If the total maneuver time can be chosen to be a multiple of the beat period, the boom oscillations at the end of the maneuver can be reduced. The beat period is equal to the precession period of the boom hub in inertial space for the third mode calculated by Eq. 24. The total maneuver time can be fine tuned by varying the pulse time as shown in Eq. 34. One limitation to this approach, however, is that uncertainties in the system parameters and thruster performance will introduce uncertainties in the beat period. Since the oscillations excited during the maneuver are linearly proportional to the average torque, a second approach to mitigate boom oscillations at the end of a maneuver is to reduce the average torque by using smaller

	Mode #	1	2	3	4	5	f
ω_i/Ω		1.0145	1.0118	1.0470	1.0135	0.4496	1
z	m	0	0	0	0	0	0
ω_x	rad/sec	0	0	4.0e-4(-.33)	4.7e-4(.35)	4.1e-3(-1.55)	9.7e-4(2.69)
ω_y	rad/sec	0	0	2.5e-3(-.16)	4.7e-4(-1.20)	3.2e-3(-3.12)	1.0e-3(1.01)
ϕ_1	rad	0	0	7.7e-2(-.63)	1.1e-2(2.53)	4.6e-3(.94)	6.8e-2(2.53)
ϕ_2	rad	0	0	7.3e-2 (.98)	8.9e-3(.96)	5.5e-3(-1.20)	8.3e-2(-2.18)
ϕ_3	rad	0	0	7.7e-2 (2.51)	1.1e-2(-.61)	4.6e-3(-2.20)	6.8e-2(-.61)
ϕ_4	rad	0	0	7.3e-2 (-2.16)	8.9e-3(2.18)	5.5e-3(1.94)	8.3e-2(.96)

Table 10. Repointing Maneuver Forced Response Magnitudes (Phases)

pulses for the maneuver. A drawback to this approach, however, is an increase in total thrusting time and number of valve cycles.

V. Simulation Results

The results of the linear analysis above were found to correlate very closely to simulations done using a full nonlinear model. This model was created using the SimMechanics©package, a commercial add-on to Matlab's Simulink©software. SimMechanics allows systems to be defined using rigid bodies connected by joints. The nonlinear dynamics of the system are automatically derived inside the software from the parameters defined by the user. Thus, the linearized dynamics from the analysis above were derived independently from the dynamics in the simulation. In addition to running the full nonlinear dynamics, the simulation model had several other differences from the linearized model above. First, the booms were modeled using multiple links with distributed mass that rotate both in and out of the spin plane. The nonlinear model also included fuel slosh, solar torques and gravitational effects. The repointing maneuvers in the simulation were performed using discrete thruster pulses timed off of a simulated sun pulse. Although more complicated damping models including coulomb friction were incorporated into the nonlinear model, the simulation results presented here were from runs with only viscous damping enabled.

In the first simulation, an initial condition was chosen to excite all of the modes of the system. The frequency response is illustrated in Fig. 4. The response was calculated by taking the FFT of the response of boom 1, ϕ_1. The frequencies were normalized by the spin rate Ω. These results illustrate the presence of five dominant peaks in the response of the nonlinear system that correspond well to the five frequencies predicted by the linear analysis. Further, the results confirmed that oscillations along the booms were negligible because angular deflection of the joints along the simulated booms were far less than the deflections at the root.

In the second group of analyses, five unforced simulations were run with the initial conditions corresponding to each of the mode shapes found from the linear model. For each of the mode shapes, the initial values of each variable were set to the real parts of the mode shapes in Table 5 scaled by constant. For the booms, the initial angular rates, $\dot{\phi}_i(0)$, were calculated from the imaginary parts of the mode shapes in Table 5. This was done using the relationship:

$$y(t) = (\alpha + \beta j)e^{j\omega_i t} \Rightarrow \dot{y}(t) = (-\beta\omega_i + \alpha j\omega_i)e^{j\omega_i t} \tag{38}$$

Thus, the real part of the velocity is dependent on the imaginary part of the position. The same damping properties in Table 6 were used in the simulation. In each of these five simulations, the responses were exponentially decaying single frequency sinusoids validating that the initial conditions were in fact mode shapes of the system. Figure 5 illustrates the simulated response for each mode for one of the boom angles, ϕ_i, compared to the analytically estimated exponential envelopes from the time constants calculated in Table 7.

A third test simulated an axial thrust on the central hub of the system. The simulated response in Fig. 6, illustrates that the resulting boom angles were quite small as predicted in Table 9. The responses of boom 3 was identical to the response of boom 1, and the response of boom 4 was identical to the response of boom 2, confirming that the only the first two mode shapes were excited.

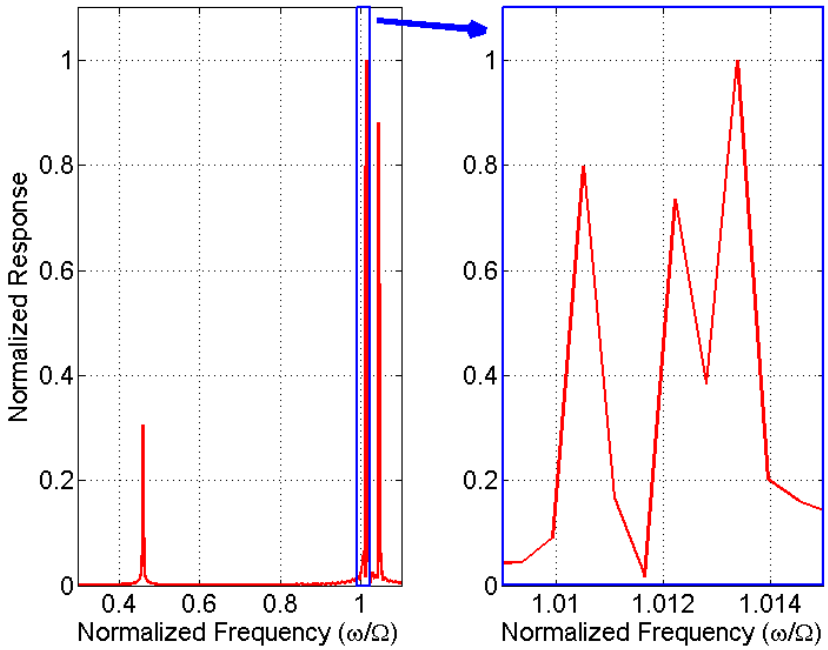

Figure 4. Unforced Frequency Response

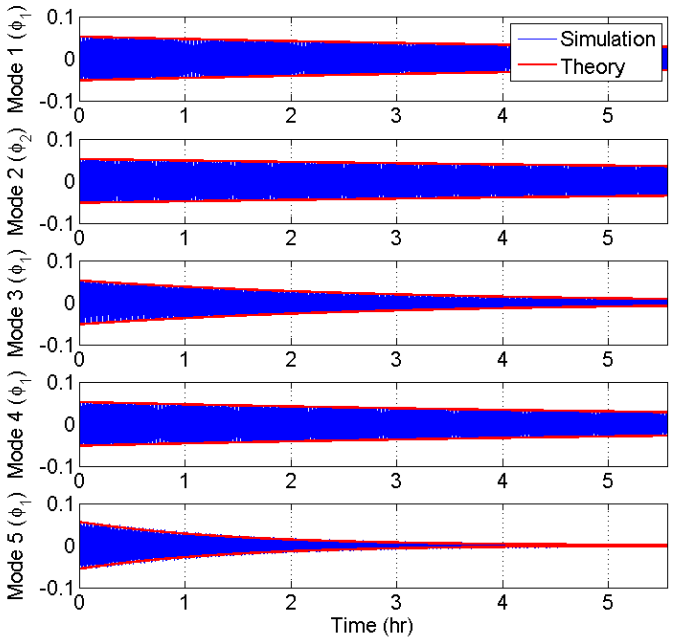

Figure 5. Decay of Single Mode Response

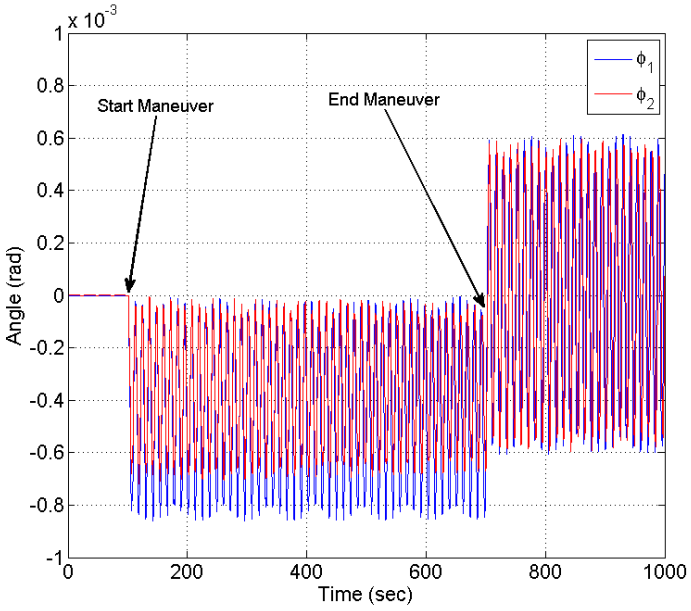

Figure 6. Axial Thrust Maneuver Boom Angle Response

The final test simulated a repointing Rhumb line maneuver maintaining a constant angle with respect to the sun vector. The boom responses for the first two booms are illustrated in Fig. 7. The beat frequency seen during the maneuver closely matches the one predicted analytically in Table 10. The maximum boom angles seen in the simulation are approximately equal to the sum of the magnitudes of the analytical responses for mode 3 and the mode at the forcing frequency. In order to better visualize the maneuver, Fig. 8 shows the trace of the hub z axis vector and the normal vector to the boom plane on a unit sphere, illustrating the mutual precession of these two vectors.

VI. Conclusion

A linearized model for the out-of-plane dynamics of a spinning spacecraft with four flexible wire boom appendages has been presented. This model was used to predict the mode shapes, frequencies, and damping of the system. The frequencies and mode shapes for the three gyroscopically coupled modes of the four boom configuration have not been correctly identified in previous studies.[3,4] The analytical model was also used to predict the forced response for both an axial ΔV maneuver and a repointing maneuver characteristic of planned maneuvers for the RBSP spacecraft. The axial ΔV maneuver was found to produce negligible oscillations in the system. The repointing maneuver was found to excite beating between one of the gyroscopically coupled modes and a second forced mode at the spin frequency. Two methods for mitigating the effects of the excited oscillations were presented including timing the maneuver to end at a low point in the beating response or using smaller average torque to reduce the maximum oscillations. An independent nonlinear simulation confirmed the validity of the linearized model.

Acknowledgments

The overall GNC effort for the RBSP spacecraft was lead by Robin Vaughan. Hollis Ambrose and Brian Kemp provided the nonlinear simulations used to verify analytical results. Testing to characterize damping properties in the boom wires was performed at the University of California, Berkeley by D. Pankow, G. Dalton, P. Turin and J. Bonnell. This work was sponsored by NASA under contract NNN06AA01C.

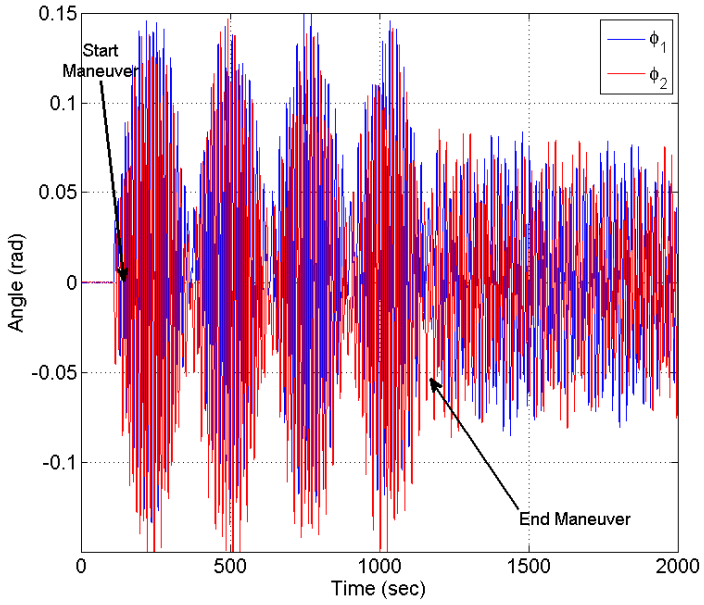

Figure 7. Repointing Maneuver Boom Angle Response

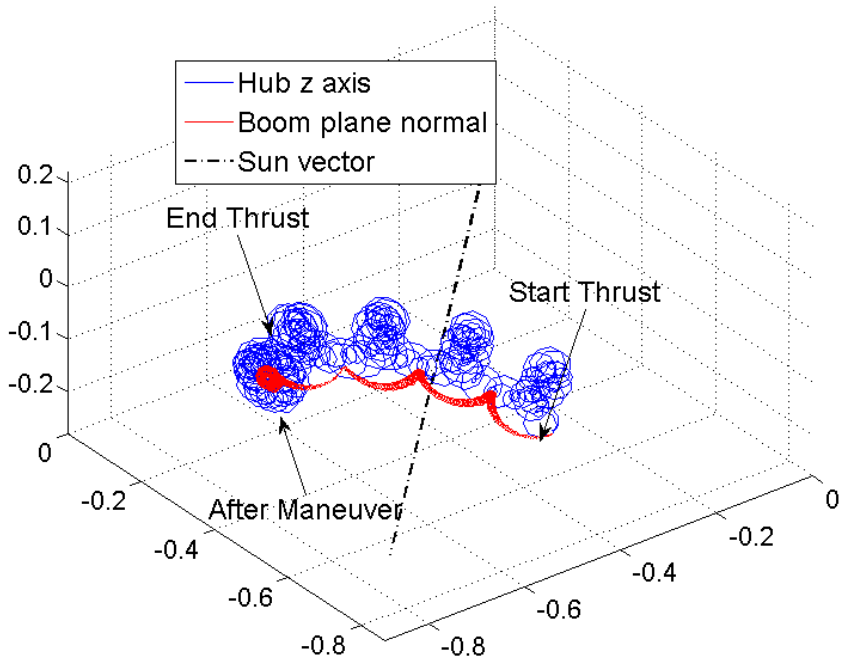

Figure 8. Inertial Trace of Spacecraft z Axis and Boom Plane Normal

References

[1]Kemp, B. L., McGee, T. G., and Shankar, U. J., "Analysis of Spinning Spacecraft with Wire Booms, Part 1: Derivation of Nonlinear Dynamics," *accepted to the AIAA Guidance, Navigation, and Control Conference*, 2009.

[2]Shankar, U. J., McGee, T. G., and Kemp, B. L., "Analysis of Spinning Spacecraft with Wire Booms, Part 3: Spin-Plane Dynamics, Maneuvers, and Deployment," *accepted to the AIAA Guidance, Navigation, and Control Conference*, 2009.

[3]Longman, R. W. and Fedor, J. V., "Dynamics of Flexible Spinning Satellites with Radial Wire Antennas," *Acta Astronautica*, Vol. 3, 1976, pp. 17–37.

[4]Lai, S. T. and Bhavnani, K., "Dynamics of Wire-Boom Systems," AFRL Report TR-75-0220, AFCRL, 1975.

[5]Vogel, E., "Multipulse Precession of Spinning Spacecraft with Flexible Appendages," AIAA-1980-1782, 1980.

[6]Chen, J. and You, D., "Hysteretic Damping Revisited," *Advances in Engineering Software*, Vol. 28, 1997, pp. 165–171.

[7]Chen, K. and Zhang, S., "On the Impulse Response Precursor of an Ideal Linear Hysteretic Damper," *Journal of Sound and Vibration*, Vol. 312, 2008, pp. 576–583.

[8]Shankar, U., Kemp, B., Ambrose, H., and Vaughan, R., "Design and Analysis of Passive Dampers for the RBSP Spacecraft," *AIAA/AAS Astrodynamics Specialist Conference and Exhibit Honolulu, HI, AIAA-2008-6601*, 2008, pp. 1–25.

[9]Hubert, C., "Modeling Completely Filled Viscous Ring Nutation Dampers," GSFC Technical Report B2027, Hubert Astronautics, Inc., 2002.

[10]Wertz, J. R., editor, *Spacecraft Attitude Determination and Control*, R. Reidel Publishing Company, 1978.